Published online 21 February 2017 *Nucleic Acids Research, 2017, Vol. 45, No. 10* ***5691–5706***
doi: 10.1093/nar/gkx131

H3.Y discriminates between HIRA and DAXX chaperone complexes and reveals unexpected insights into human DAXX-H3.3-H4 binding and deposition requirements

Lisa-Maria Zink[1], Erwan Delbarre[2], H. Christian Eberl[3], Eva C. Keilhauer[3], Clemens Bönisch[1], Sebastian Pünzeler[1], Marek Bartkuhn[4], Philippe Collas[2], Matthias Mann[3,5] and Sandra B. Hake[1,4,5,*]

[1]Department of Molecular Biology, BioMedical Center, Ludwig-Maximilians-University Munich, 82152 Planegg-Martinsried, Germany, [2]Department of Molecular Medicine, Institute of Basic Medical Sciences, Faculty of Medicine, University of Oslo, 0317 Oslo, Norway, [3]Department of Proteomics and Signal Transduction, Max-Planck-Institute of Biochemistry, 82152 Martinsried, Germany, [4]Institute for Genetics, Justus-Liebig-University Giessen, 35392 Giessen, Germany and [5]Center for Integrated Protein Science Munich (CIPSM), 81377 Munich, Germany

Received July 27, 2016; Revised January 20, 2017; Editorial Decision February 13, 2017; Accepted February 14, 2017

ABSTRACT

Histone chaperones prevent promiscuous histone interactions before chromatin assembly. They guarantee faithful deposition of canonical histones and functionally specialized histone variants into chromatin in a spatial- and temporally-restricted manner. Here, we identify the binding partners of the primate-specific and H3.3-related histone variant H3.Y using several quantitative mass spectrometry approaches, and biochemical and cell biological assays. We find the HIRA, but not the DAXX/ATRX, complex to recognize H3.Y, explaining its presence in transcriptionally active euchromatic regions. Accordingly, H3.Y nucleosomes are enriched in the transcription-promoting FACT complex and depleted of repressive post-translational histone modifications. H3.Y mutational gain-of-function screens reveal an unexpected combinatorial amino acid sequence requirement for histone H3.3 interaction with DAXX but not HIRA, and for H3.3 recruitment to PML nuclear bodies. We demonstrate the importance and necessity of specific H3.3 core and C-terminal amino acids in discriminating between distinct chaperone complexes. Further, chromatin immunoprecipitation sequencing experiments reveal that in contrast to euchromatic HIRA-dependent deposition sites, human DAXX/ATRX-dependent regions of histone H3 variant incorporation are enriched in heterochromatic H3K9me3 and simple repeat sequences. These data demonstrate that H3.Y's unique amino acids allow a functional distinction between HIRA and DAXX binding and its consequent deposition into open chromatin.

INTRODUCTION

In eukaryotes, epigenetic information is stored, stabilized and organized in form of chromatin (1). This large polymer consists of 145–147 base pairs of DNA wrapped around an octamer of proteins, consisting of two of each histones H2A, H2B, H3 and H4 (2). Besides these canonical histones, so-called histone variants have evolved that differ in amino acid sequence, post-translational modification (PTM) pattern and sometimes even structure (3). In contrast to replication-dependent canonical histones, most histone variants are transcribed in a replication-independent manner, at all stages of the cell cycle. To ensure epigenetic inheritance, histones have to be faithfully distributed at sites of naked DNA when needed, for example during or after replication, transcription or DNA damage repair (4). In mammals, histone variants of the H3, H2A and H2B families have been identified, all involved in distinct bio-

*To whom correspondence should be addressed. Tel: +49 641 99 35460; Fax: +49 641 99 35469; Email: sandra.hake@gen.bio.uni-giessen.de
Present addresses:
H. Christian Eberl, Cellzome GmbH, a GSK company, Meyerhofstrasse 1 69117 Heidelberg, Germany.
Clemens Bönisch, Vertex Pharmaceuticals (Germany) GmbH, Sonnenstrasse 19, 80331 Munich, Germany.
Sebastian Pünzeler, Coparion GmbH & Co. KG, Charles-de-Gaulle-Platz 1d, 50679 Cologne, Germany.

logical processes. The human histone H3 family consists of H3.1 and H3.2, both expressed during S-phase but enriched with distinct PTMs (5,6), the evolutionary conserved histone variant H3.3, testis-specific H3.1t and H3.5 variants and the centromere-determinative CENP-A (CenH3). Recently, we have discovered a primate-specific H3 variant, which we termed H3.Y (H3.Y.1) (7,8). H3.Y is predominantly expressed in different human brain regions, some tumor tissues and is upregulated by stress stimuli. Interestingly, H3.Y is mainly found in euchromatic regions and seems to be involved in the expression of genes involved in cell cycle control (7).

Faithful chromatin deposition of histone variants in a spatial- and temporally-restricted manner is accomplished by specialized chaperones and chromatin remodeling complexes (9,10). While newly synthesized H3.1 and H3.2 are reassembled on DNA after replication and non-homologous end joining by the three-subunit protein complex CAF-1 (Chromatin-Assembly Factor 1) (11), deposition of H3.3 is more complex. The HUCA (HIRA/UBN1/CABIN1/ASF1a) complex places H3.3 in transcriptionally active genic regions (11,12) and at sites of DNA repair (13). In contrast, the DAXX/ATRX (death-domain associated protein/α Thalassemia/Mental Retardation X-linked) complex is responsible for H3.3 deposition at repetitive heterochromatic regions (14–16) including telomeres (17) in mouse ESCs (embryonic stem cells). Interestingly, DAXX/ATRX are often mutated, in addition to H3.3, in pediatric glioblastomas (reviewed in (18)). However, while much is known on the assembly of H3.3 into chromatin, the chaperones and mechanism(s) responsible for H3.Y deposition are unknown.

Here, we report the identification and biochemical characterization of H3.Y-specific chaperone complexes. We show that, as expected from the shared and conserved chaperone recognition site motif in H3.3 and H3.Y, HIRA and other members of the HUCA complex interact with chromatin-free nuclear H3.Y. Accordingly, we find nucleosomal H3.Y to be associated with euchromatic factors and depleted of repressive PTMs. Surprisingly, the DAXX/ATRX complex is not able to bind H3.Y, explaining its exclusive euchromatic localization, its strong correlation with H3K4me3 sites and its inability to localize to PML-NBs (promyelocytic leukemia-nuclear bodies). H3.Y mutational analyses and *in vivo* chaperone binding assays reveal the dependence of DAXX interaction and PML-NB recruitment to a combination of some few H3 core and C-terminal amino acids. Restoration of H3.Y DAXX-binding ability leads to deposition at heterochromatic H3.3-specific and H3K9me3-enriched simple repeat sequences. Our data provide compelling evidence that HIRA-dependent H3.Y deposition accounts for its function in gene activation. They further provide new insights into an unexpected DAXX-H3.3 combinatorial binding mode and human DAXX/ATRX-recruitment DNA sequence requirements.

MATERIALS AND METHODS

Cell culture, transfection and flow cytometry

Hela Kyoto (HK) cells were grown in Dulbecco's modified Eagle's medium (DMEM) (Sigma) supplemented with 10% fetal calf serum (FCS; Sigma) and 1% penicillin/streptomycin at 37°C and 5% CO_2. Transfection was performed as described in (19) using X-tremeGene (Roche Applied Science) according to the manufacturer's instruction. Expression levels of HK cells stably transfected with eGFP and eGFP-tagged histone H3 variants and mutants were quantified using a FACSCanto machine (Becton Dickinson). Human primary mesenchymal stem cells were purified from lipoaspirates and cultured and transfected by electroporation using Nucleofector™ Technology (Lonza) as described in (20).

Plasmids

For expression in human cells, H3 variant cDNA was cloned into a pIRESneo-EGFP plasmid that was generated from pIRESneo (digested with EcoRV and and BamHI) with the EGFP insert from pEGFP-C1 (digested with NheI followed by Klenow reaction and subsequently digested with BamHI). Single point mutations in eGFP-H3.Y were introduced using site-directed mutagenesis with the following primers: H3.YQ59E: 5′- CCAGAAGTCCACGGAG CTGTCC-3′,

H3.YDFKT: 5′- CGAGATCGCCCAGGATTTCAAA ACCGACCTGCGCTTCC-3′,

H3.YQ102G: 5′- GAGGCCTACCTGGTGGGTCTCT TTGAAGACACC-3′,

H3.Y K42R K53R core C3:
5′-GATCAAGAAGCCTCACCGCTACAGGCCTGG CACCCTGGCGCTGCGGG-3′,

H3.Y L46V K53R core C3:
5′-TACAAGCCTGGCACCGTGGCGCTGCGGGAA ATC-3′,

H3.Y K53R L62I core C3:
5′-GAAGTCCACGGAGCTGCTCATTCGCAAGCT GCCCTTCCAG-3′,

H3.Y K42R L46V K53R core C3:
5′-GATCAAGAAGCCTCACCGCTACAGGCCTGG CACCGTGGCGCTGCGGG-3′.

Briefly, polymerase chain reaction (PCR) reaction was performed under standard conditions with 20 cycles, the template plasmid DpnI digested and the newly amplified plasmid containing the desired mutations was transformed into Stellar bacteria (Clontech). Tail swap mutant sequences and H3.Y core C-terminal mutants were generated by GENEWIZ and cloned into pEGFP-IRES-neo using a commercial gateway cloning system (Thermo Fisher) according to manufacturer's instructions. Correct sequences of all DNA products established by cloning or by PCR-induced mutagenesis were verified by sequencing (MWG).

Antibodies

The following commercially available antibodies were used: α-DAXX (clone M-112, order number SC-7152; Santa

Cruz; and clone 25C12, order number 45335; Cell Signalling), α-GFP (order number 11814460001; Roche, for immunoblotting; and order number ab290, abcam, for chromatin immunoprecipitation (ChIP)), α-H3K9me3 (order number C15410003; Diagenode), α-PML (ordering number ab53773; Abcam), α-H3S10ph (order number ab39253; Active Motif). The following secondary antibodies were used: α-rabbit-HRP and α-mouse-HRP (order number rabbit: NA934; mouse: NA931, VWR), α-mouse-Alexa Fluor 555 (order number: A21424; Invitrogen).

Stable isotope labeling with amino acids in cell culture (SILAC) and mass spectrometric identification of histone chaperone complexes

HK cells stably expressing enhanced green fluorescence protein (eGFP)-tagged H3 variants were SILAC labeled and nuclear extracts prepared as described in (19,21,22). Briefly, extracts were diluted in incubation buffer (150 mM NaCl, 50 mM Tris–HCl pH 8.0, 0,25% NP40) supplemented with complete protease inhibitors w/o ethylenediaminetetraacetic acid (EDTA) (Roche) and 0.5 mM Dithiothreitol (DTT) to a concentration of 1.5 μg/μl. A total of 400 μl solution were incubated with GFP-trap magnetic beads (Chromotek) for 3 h at 4°C. After washing for three times with 1 ml incubation buffer, precipitates were combined and eluted by boiling in 2× loading buffer. Samples were loaded on 1D NuPAGE gels (Invitrogen), lanes cut into eight stripes, in-gel digested with trypsin and desalted by stage tipping. High-resolution LC MS/MS analysis was done on an LTQ Orbitrap mass spectrometer as described before (19,22). Peptides were separated using an easy nano-LC system (Proxeon Biosystems) and the MS operated as described in detail in (19) (see Supplementary Tables S1–3 for all identified interactors).

Preparation of chromatin-free extracts, immunoprecipitation and immunoblot analysis of H3.3 mutant HK cell lines

HK cells stably expressing eGFP-tagged H3 variants and eGFP-H3.Y mutant cell lines were used for preparation of chromatin-free extracts. Nuclear extracts were prepared as described in (19,21,22), ultracentrifuged at 186000 rcf and total protein concentration of the supernatant was determined by Bradford assay (Biorad), according to the manufacturer's instructions. 400–1500 μg of total protein to fit the respective eGFP expression levels as determined by flow cytometry analyses were diluted to a final concentration of 210 mM NaCl and used for immunoprecipitation with GFP-trap magnetic beads (Chromotek). After rotating for 2 h at 4°C, samples were washed five times with 500 μl wash buffer (50 mM Tris–HCl pH 7.5, 150 mM NaCl, 1× complete protease inhibitors w/o EDTA (Roche), 0.5 mM DTT, 0.01% NP40). Samples were then boiled in 2× loading buffer, proteins separated with SERVAGelTG PRIME 4–12% sodium dodecyl sulphate-polyacrylamide gel electrophoresis (SDS-PAGE) gels (Serva), followed by immunoblotting.

Label-free mass spectrometric identification of H3 nucleosome binding proteins

Mononucleosomes for label-free mass spectrometry (MS) or immunoblot analyses were isolated as described previously (23) and the supernatant 1 (S1) fraction was used for immunoprecipitation (IP) experiments. Mononucleosome immunoprecipitations, LC-MS/MS analysis and MS raw data analysis were basically carried out as previously described (24). After IP, proteins bound to the GFP-trap beads (Chromotek) were eluted by overnight digestion with trypsin (Promega). The resulting peptides were purified and concentrated on C18 StageTips (25).

For LC-MS/MS analysis, peptides were eluted from the C18 StageTips according to the standard protocol (25) and analyzed by reversed-phase liquid chromatography on an EASY-nLC 1000 system (Thermo Fisher Scientific, Odense, Denmark) coupled to a Q Exactive mass spectrometer (Thermo Fisher Scientific). HPLC columns of 20 cm length and an inner diameter of 75 μm were in-house packed with ReproSil-Pur 120 C18-AQ 1.9 μm particles (Dr Maisch GmbH, Germany). Peptide mixtures were separated using linear gradients of 140 min (total run time + washout) and a two buffer system: buffer A++ (0.1% formic acid) and buffer B++ (80% acetonitrile in 0.1% formic acid). The flow rate was set to 250 nl/min and the column was heated to 50°C using a column oven (Sonation GmbH, Germany). Peptides eluting from the column were directly sprayed into the mass spectrometer with a spray voltage of 2.4 kV and a capillary temperature of 250°C. The mass spectrometer was operated in a data-dependent mode acquiring survey scans at a resolution of 70 000 with an automatic gain control (AGC) target of 3E06 ions and a maximum ion injection time of 20 ms. Subsequently the top 10 most abundant peaks were selected for fragmentation with an isolation window of 2 m/z and fragmented by higher energy collisional dissociation with a normalized collision energy of 25. Fragmentation spectra were acquired at a resolution of 17 500 with a target value of 1E05 ions and 120 ms maximum ion injection time. The dynamic exclusion feature was enabled within a time window of 20 s to minimize re-sequencing of peptides.

MS raw data were processed using the MaxQuant software (26) version 1.3.9.20. Fragmentation spectra were searched against a human sequence database obtained from Uniprot in May 2013 and a file containing frequently observed contaminants such as human keratins. Cysteine carbamidomethylation was set as a fixed modification; N-terminal acetylation and methionine oxidation were set as variable modifications. Trypsin was chosen as specific enzyme, with two maximum missed cleavages allowed. Peptide and protein identifications were filtered at a 1% false discovery rate (FDR). Label-free quantification was enabled, with a minimum ratio count of one. The match between runs option was enabled with a matching time window of 0.5 min and an alignment time window of 20 min, while the requantify option was disabled. All other parameters were left at standard settings.

MaxQuant output tables were analyzed in Perseus (27) version 1.5.3.0 essentially as described in (28). After deleting proteins only identified with modified peptides, hits

to the reverse database, contaminants and proteins with one or less razor and unique peptides, label-free intensities were log2 transformed. Next, proteins were required to have three valid values in at least one triplicate, then remaining missing values in the data matrix were imputed with values representing a normal distribution around the detection limit of the mass spectrometer. Now a two-sample *t*-test was performed to identify proteins enriched (*t*-test difference > 0) in the 12 histone pulldowns compared to the three eGFP controls. Only those proteins were kept for further analysis. Then, two-sample *t*-tests were performed comparing H3.2 versus H3.1, H3.3 versus H3.1, H3.Y versus H3.1 and H3.Y versus H3.3. Significant outliers were determined using a permutation-based FDR. The S0 and FDR parameters were adjusted for each *t*-test (see Supplementary Tables S5–9), the number of permutations was always 250. The respective *P*-values (technical replicates) and *t*-test differences were plotted against each other in volcano plots using R version 2.15.3. In addition to the volcano plots, interacting proteins were also visualized in heatmaps. To do so, the ratio (fold change) of the logarithmized and averaged triplicate LFQ intensities of eGFP-tagged H3 histone mononculeosomes were plotted as heatmaps using Perseus.

Fluorescence microscopy of cells and chromosomes

Preparation of HK cells and chromosome spreads for fluorescence microscopy was done as previously reported (29). Briefly, wide-field fluorescence imaging was perfomed with a PersonalDV microscope system (Applied Precision) equipped with a 60x/1.42 PlanApo oil objective (Olympus), CoolSNAP ES2 interline CCD camera (Photometrcis), Xenon illumination and appropriate filter sets.

Chromosome spreads were analyzed by confocal imaging using the TCS Leica SP5 II microscope system with a 63x/1.3 PL APO glycerol immersion objective and lasers with excitation lines of 405 nm (4,6-diamidino-2-phenylindole (DAPI)) and 488 nm (GFP).

Mesenchymal stem cells grown on coverslips were fixed for 15 min with 3% paraformaldehyde in PBS, 24 h after transfection. After three PBS washes and a 30 min block with PBS/Tween 20 (0.01%)/Triton Tx-100 (0.1%)/bovine serum albumin (BSA, 2%), coverslips were incubated with the primary antibody for 45 min, washed three time in PBS/Tween 20 (0.01%)/BSA (2%) and incubated with the secondary antibody for 45 min. Cells were then washed three times in PBS and DNA was labeled with 0.25 mg/ml DAPI in PBS for 5 min. Coverslips were mounted in Mowiol 4–88 (Polysciences). Images were acquired on an Olympus IX71 upright microscope fitted with the DeltaVision system (Applied Precision-GE Healthcare), and processed with ImageJ 1.42q.

ChIP-seq

Chromatin Immunoprecipitation. HK cells stably expressing eGFP or eGFP-tagged H3.3, H3.Y, N3-Y, NY-3, 3-CY, Y-C3 or H3.Y L46V K53R L62I core C3 were fixed with 1% formaldehyde in DMEM at a density of 2×10^6 cells/ml. After quenching with 125 mM glycine cells were washed 3× with PBS containing 10% FCS and flash frozen. Fixed cells were resuspended in 5 ml lysis buffer 1 (50 mM Hepes-KOH, pH 7.5, 140 mM NaCl, 1 mM EDTA, 10% glycerol, 0.5% NP-40, 0.25% Triton X-100, protease inhibitors w/o EDTA (Roche)) and incubated at 4°C for 10 min. After centrifugation for 5 min at 1350 × *g*, the pellet was resuspended in lysis buffer 2 (10 mM Tris–HCl, pH 8.0, 200 mM NaCl, 1 mM EDTA, 0.5 mM EGTA, 1 × protease inhibitors), incubated for 10 min at room temperature and spun down. For chromatin shearing the pellet was resuspended in buffer B (50 mM Tris–HCl, pH 8.0, 10 mM EDTA, 0.5% SDS) and subjected to Covaris S220 (PIP 120 W, DF 20%, 200 CB, 35 min) to generate chromatin fragments of 150 bp in average size. The sheared DNA was centrifuged for 10 min at 18 400 × *g* at 4°C. Subsequently 9 ml ice cold buffer A (10 mM Tris–HCl, pH 7.5. 1 mM EDTA, 0.5 mM EGTA, 1% Triton X-100, 0.1% SDS, 0.1% Na-deoxycholate, 140 mM NaCl, 1 × protease inhibitors) was added to the soluble fraction. A total of 1 ml aliquots were used for immunoprecipitations with α-GFP antibody bound to Dynabeads. For beads-antibody coupling, 30 μl Dynabeads M-280 Sheep Anti-Rabbit IgG (Novex) were washed 2× with 500 μl 0.1% PBS-Tween. Next, 5 μg α-GFP antibody (Abcam) was bound to the beads by incubating for at least 2 h at 4°C while rotating. Beads were washed 2× with 0.1% PBS-T. Immunoprecipitations were carried out with 1 ml sheared chromatin at 4°C, rotating at 7 rpm o/n. The following day, the beads were collected, washed 4× with ice cold buffer A and 1× with ice cold buffer C (10 mM Tris–Hcl, pH 8.0, 10 mM EDTA). Afterward, beads were resuspended in 100 μl elution buffer (50 mM Tris–HCl, pH 8.0, 10 mM EDTA, 1% SDS) and incubated at 65°C o/n with 750 rpm shaking. After magnetic separation, the supernatant was transferred into a fresh tube, 100 μl Tris-EDTA (TE) and 4 μl RNaseA (10 mg/ml) were added and incubated at 37°C for 1 h. Next, 4 μl Proteinase K (10 mg/ml) was added and the reaction was incubated at 56°C for 2 h. DNA was purified using the QIAGEN MinElute PCR Purification Kit (QIAGEN) following the manufacturer's instructions and eluted in 30 μl elution buffer. To determine DNA concentrations the Qubit dsDNA hs Kit (Invitrogen) was used. Illumina Sequencing libraries were created with the MicroPlex Library Preparation Kit (Diagenode) following the manufacturer's protocol. DNA was eluted in 20 μl 0.1× TE, pH 8.0.

Illumina sequencing. Next-generation sequencing was performed by Dr. Stefan Krebs at the Laboratory of Functional Genome Analysis (LAFUGA) in Munich (Gene Center). Libraries were sequenced on an Illumina HiSeq 2000 using V3 clustering and sequencing reagents (50 bp read length) according to manufacturer's instructions.

ChIP-seq analysis. Quality control of FASTQ files was done using *fastqc* (http://www.bioinformatics.babraham.ac.uk/projects/fastqc/). No additional trimming or filtering was applied. Additional publicly available chromatin immunoprecipitation sequencing (ChIP-seq) data were downloaded from NCBI's Gene Expression Omnibus (GEO). Raw reads were downloaded as SRA archives and were extracted into FASTQ files using the *fastq-dump* program of the NCBI *SRA Toolkit* (https://trace.ncbi.nlm.nih.gov/Traces/sra/).

Publicly available data used in this study:

H3K9me3 ChIP-seq data from HeLa cells: sample GSM2308949 from GSE86811

H3K4me3 ChIP-seq coverage data from HeLa cells: ENCODE data downloaded trough the UCSC genome browser portal (http://hgdownload.cse.ucsc.edu/goldenpath/hg19/encodeDCC/wgEncodeBroadHistone/wgEncodeBroadHistoneHelas3H3k4me3StdSig.bigWig)

Reads were aligned with Bowtie 2 (30) as previously described (31). Parameter settings were *bowtie2-align -p 6 -D 15 -R 2 -N 0 -L 32 -i S,1,0.75 -M 10000*. Repeat information was downloaded through the hg19 table browser of the UCSC genome browser. Peaks were called using MACS version 2 (32) with default settings. If not indicated differently, all downstream analyses were done in R/BioConductor (33). Neighboring peaks were stitched together when lying within 2 kb. When available, the overlap between two replicates was then selected as the actual set of binding sites for downstream analysis. Hg19 RefSeq annotations were downloaded from Illumina's iGenome repository. In order to identify H3.3 sites bound differentially for H3.Y, extended reads (200 bp) were counted across these intervals. DESeq2 was used for normalization of read counts as well as for inference of regions with relevant binding differences between H3.3 and H3.Y (34). DESeq2-normalized read counts were further normalized for peak width and then used in order to visualize differential binding efficiencies between individual H3.Y-mutants. Statistical testing of observed differences was done using Wilcoxon-signed-rank test. *De novo* discovery of enriched motifs within sites with reduced H3.Y binding was done with MEME-ChIP (35). Coverage vectors were produced using deepTools *bamCoverage* function. Similarly, deepTools was used for representation of ChIP-seq coverage across peak intervals as heat maps (36). Bigwig files were used for visualization via the R/BioC-package Gviz (37).

RESULTS

H3.Y binds to HIRA but not DAXX/ATRX chaperone complexes

H3.Y differs from H3.1, H3.2, and H3.3 by 30, 29 or 26 amino acids, respectively, and strikingly contains the H3.3-specific chaperone-recognition sequence, encompassing amino acids 87–90 (Figure 1A). Based on H3.Y's similarity to H3.3, we suspected that identical chaperone complexes might bind to both variants. To test this hypothesis, we employed a quantitative MS-based approach, similar to the one we previously used to successfully identify chaperone complexes of the primate-specific alternative splice variant H2A.Z.2.2 (19). To do so, soluble nuclear proteins were isolated from SILAC (stable isotope labeling by amino acids in cell culture) labeled HK cells stably expressing eGFP-H3.2, eGFP-H3.3 or eGFP-H3.Y. Then, eGFP-tagged histone H3 variants were precipitated and bound proteins identified by MS (Figure 1B–D and Supplementary Tables S1–3). Whereas the majority of proteins were background binders and clustered around zero, specific H3 variant-associated proteins were seen on the lower right side of the plot. As expected, we identified all three members of the CAF-1 complex (CAF-1A, CAF-1B, CAF-1C), and the evolutionary conserved ASF1A chaperone (38) as interactors of eGFP-H3.2 (Figure 1B), verifying the applicability and specificity of our approach. Interestingly, we also found an interaction of members of the MCM2–MCM7 (mini chromosome maintenance 2–7) complex involved in DNA replication initiation and elongation (39). In agreement with a previous study (40), we also identified MCM2, MCM4, MCM6 and MCM7, but not MCM3 or MCM5 to bind to H3.2 and H3.3. As expected, we were also able to precipitate the HUCA members HIRA, CABIN1 and ASF1A, as well as DAXX and ATRX with eGFP-H3.3 (Figure 1C).

Interestingly, although we found HIRA, CABIN1, ASF1, MCM2/4/6/7, FACT80 and FACT140 to be associated with H3.Y, neither DAXX nor ATRX were identified with H3.Y (Figure 1D). This was surprising, as HUCA and DAXX have been reported to interact with the identical H3.3 core sequence (41). We therefore next verified the inability of H3.Y to recruit DAXX by an independent approach using immunoblotting (Figure 2A). Indeed, while eGFP-H3.3 was able to pull-down DAXX, eGFP-H3.Y was not. Further, we have recently shown that newly synthesized H3.3-H4 dimers are recruited to PML-NBs in a DAXX-dependent manner (20). Using fluorescence imaging of transiently transfected H3.3-GFP (20) or eGFP-H3.Y (Figure 2B), we observed that strikingly, while most H3.3 was found in PML nuclear bodies 24 h after transfection (i.e. early after synthesis of the epitope-tagged histone), most of H3.Y (>90%) was excluded from these structures (Figure 2C). This supports our finding that H3.Y is unable to bind DAXX. We conclude that chromatin-free nuclear H3.Y interacts with the H3.3-specific HIRA-containing HUCA complex, but not the DAXX/ATRX complex.

H3.Y-nucleosomes are depleted from heterochromatic H3K9me3 simple repeat regions and are bound by factors involved in transcription

Next, we determined whether binding of HIRA but not DAXX to soluble nuclear H3.Y influences its sites of chromatin deposition. We therefore performed ChIP-seq experiments using cross-linked and sonicated chromatin fragments generated from HK cells stably expressing eGFP (control), eGFP-H3.3 or eGFP-H3.Y. First, we verified the feasibility of our approach by comparing eGFP-H3.3 and eGFP-H3.Y-enriched genomic regions that were identified using MACS 2 peak-caller (32) with H3K4me3 (ENCODE data) as a marker of open and active euchromatin. Indeed, both variants and H3K4me3 peaks were enriched at genic, particularly the transcriptional start site and reduced at intergenic regions (Figure 3A). The majority of peaks were shared by both H3 variants and are indicative of open euchromatin (Figure 3B), suggesting that these sites most likely represent HIRA-mediated deposition regions (14,42,43). In agreement with this, these regions also lacked the heterochromatin mark H3K9me3 (Figure 3C). In order to identify DAXX/ATRX-dependent deposition regions we searched for H3.3-containing peaks that lacked H3.Y signal (Figure 3D). Interestingly, we detected 359 of H3.Y-reduced sites at log2-fold change <2 and adjusted *P*-value < 0.05 (see Supplementary Table S4) and observed

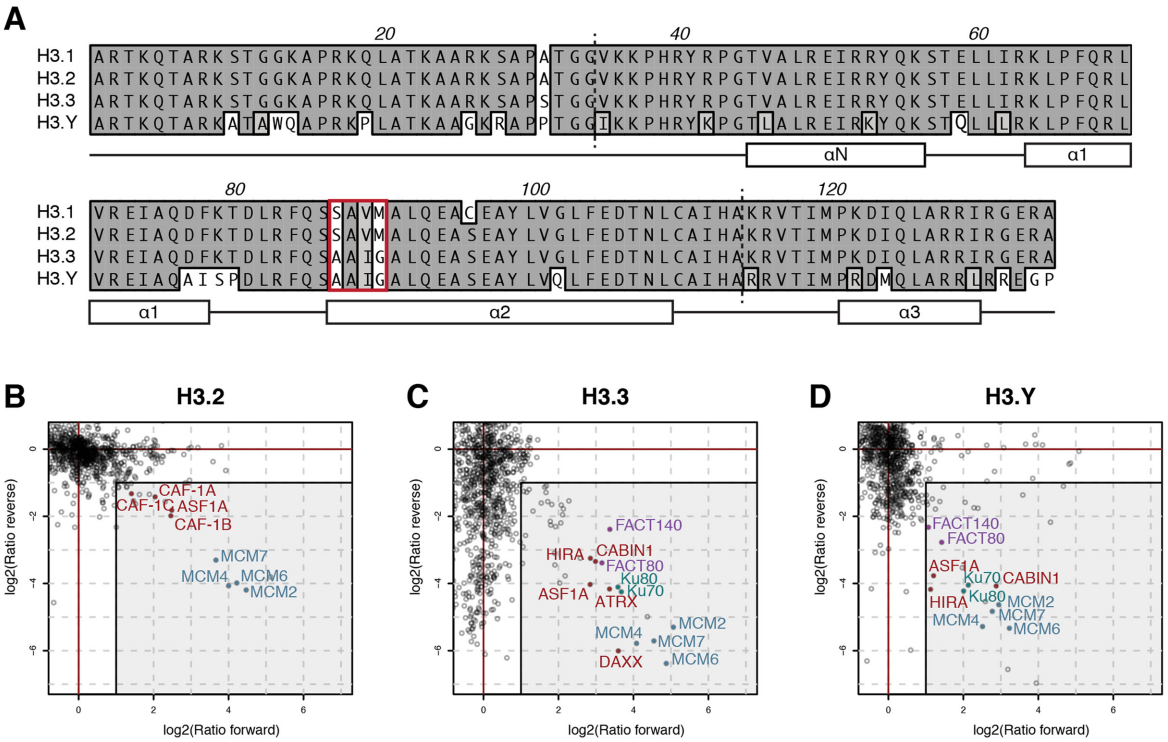

Figure 1. Identification of human H3 variant chaperone complexes. (**A**) Amino acid alignment of human H3.1, H3.2, H3.3 and H3.Y proteins using ClustalW Alignment (MacVector 13.5.1). Identical amino acids are depicted in dark gray, similar amino acids in light gray and differences are highlighted with a white background. N- and C-terminal tails are separated by dotted lines and a schematic representation of the secondary structures is shown below the alignment. The known chaperone recognition sites of H3.1, H3.2 and H3.3 are boxed. (**B**–**D**) eGFP-pull-downs for H3 variant-specific chaperone complexes are shown. HK cells stably expressing eGFP-H3.2 (B), eGFP-H3.3 (C) and eGFP-H3.Y (D) were SILAC labeled and subjected to single-step affinity purification of soluble nuclear proteins using GFP nanotrap beads. In each panel, the ratio between pull-down of the transfected cell line and a control cell line for all identified proteins after MS is plotted. Proteins known to interact with H3 variants are indicated. Background binders and potential contaminants are shown as black dots and are listed together with all identified proteins in Supplementary Tables S1–3.

that these were highly enriched in H3K9me3 (Figure 3D–F), a hallmark of DAXX/ATRX-specific heterochromatic deposition sites. Studies performed in mouse ESCs have identified such sites to be enriched in repetitive heterochromatin (14–16) including telomeres (17) and retroviral elements (44). To determine whether these potential human DAXX-dependent H3.3-deposition sites are also enriched for repeat sequences we performed a *de novo* motif search (Figure 3G). Strikingly, different simple repeats featuring guanosines and to a lesser extent thymidines are particularly enriched in H3.Y-reduced H3.3-sites. Additionally, we identified simple repeats with similar base composition as the top overrepresented repeat types overlapping with H3.Y-reduced H3.3 sites (Supplementary Figure S1). This data implies that also in humans the preferred genomic DAXX/ATRX-target sites are repetitive sequences and that H3.Y is depleted from these sites.

As a consequence, such genomic location differences between H3 variants likely result in characteristic mononucleosome interaction partners and in a distinct histone PTM pattern. To address this, chromatin isolated from HK cell lines stably expressing eGFP or eGFP-tagged H3 variants was digested with micrococcal nuclease (MNase) to generate mononucleosomes of >90% purity (Supplementary Figure S2A); nucleosomes and their associated complexes were then pulled-down using GFP nanotrap beads. Precipitated proteins from technical triplicates were trypsin digested on beads and peptides subjected to MS for identification and label-free quantification (Supplementary Tables S5–9).

After GFP-IP background filtering (Supplementary Figure S2B–D), we compared the different H3 variant nucleosome interactors with each other and depicted quantitative differences in volcano plots (Figure 4A–D). Since both H3.1 and H3.2 are deposited by CAF-1 in a replication-dependent manner, we accordingly noted no major differences in their specific nucleosome interactomes (Figure 4A). In contrast, comparison of the H3.1 versus H3.3 nucleosome-interactome revealed striking differences (Figure 4B). Not surprisingly, CAF-1A and CAF-1B were enriched on H3.1 nucleosomes. Importantly, this not only underlines the feasibility of our approach but also demonstrates association of these chaperones with both chromatin-free and chromatin-assembled H3.1/H3.2. Interestingly, DAXX, but not HIRA, was identified with H3.3 nucleosomes, suggesting a tight chromatin binding ability of DAXX but only transient mononucleosome interactions of HIRA (Figure 4B); this observation is consistent with a previous report (45). Besides DAXX, we observed a strong enrichment of H3.3. While it is probable that this corresponds to the exogenous eGFP-tagged H3.3 used for pull-downs, it is also possible that mostly homotypic H3.3 nucleosomes

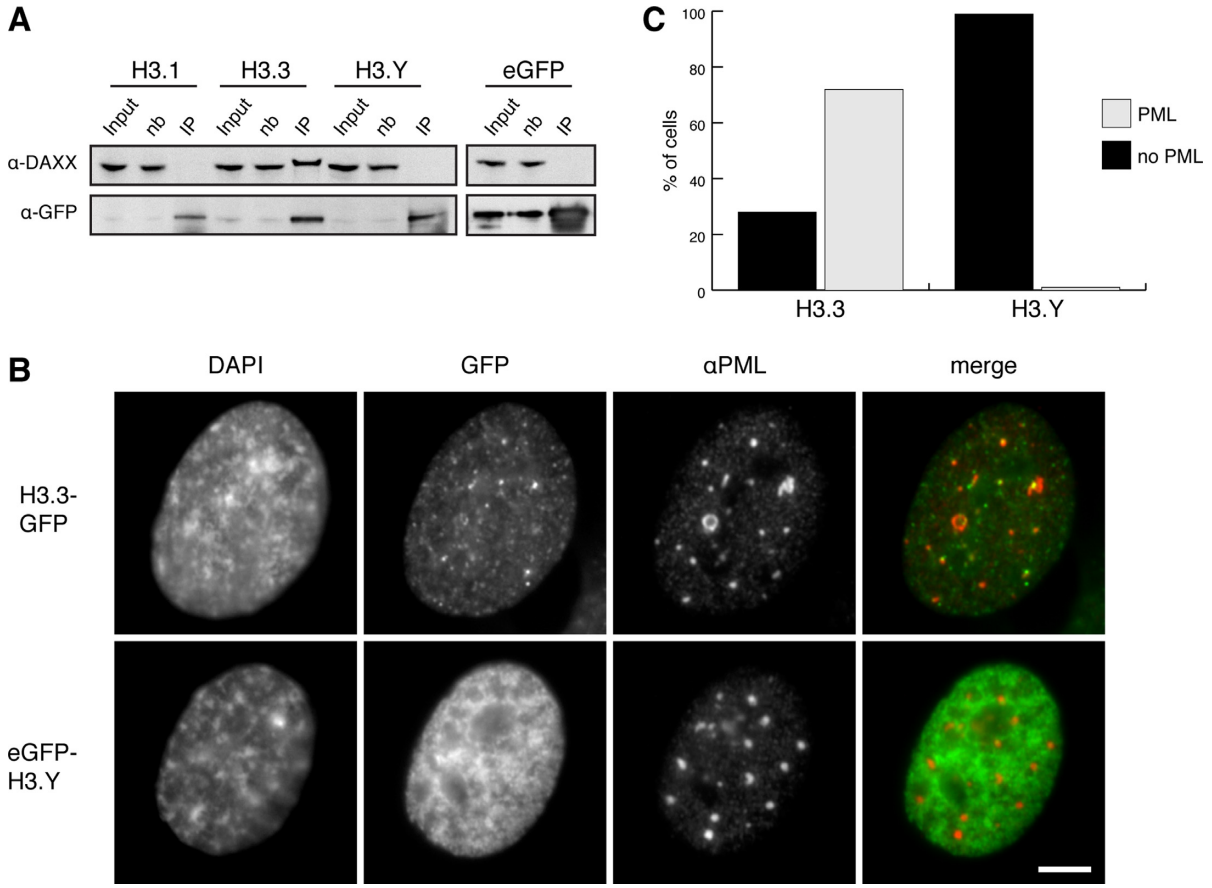

Figure 2. H3.Y prevents DAXX binding and PML body recruitment. (**A**) Soluble nuclear extracts from HK cells stably expressing eGFP, eGFP-H3.1, eGFP-H3.3 and eGFP-H3.Y were used for pull-down experiments as described in Figure 1B–D followed by immunoblotting with α-DAXX and α-GFP antibodies. Nb = non-bound fraction after precipitation, IP = immunoprecipitated material. (**B**) Immunolocalization microscopy analysis of PML, H3.3-GFP and eGFP-H3.Y in transiently transfected human primary mesenchymal stem cells. GFP: eGFP-tagged H3 variant (green); PML: α-PML antibody (red). (**C**) Percentage of cells ($n > 100$) shown in (B) exhibiting H3.3-GFP or eGFP-H3.Y PML-NB localization (gray) or not (black).

exist (supported by (11)), accounting for the observed enrichment of H3.3 peptides in MS.

Comparison of the H3.1 versus H3.Y nucleosome interactome revealed an enrichment of enzyme complexes responsible in setting repressive PTMs on H3.1, whereas H3.Y nucleosomes were enriched in proteins involved in transcription and replication (Figure 4C). H3.1-containing nucleosomes were strongly bound by the H3K9 methyltransferases SUV39H1 and SUV39H2 (suppressor of variegation 3–9 homolog 1 or 2) (46), and the H3K9me3-interacting HP1 (heterochromatin protein-1) isoforms CBX1, CBX3 and CBX5 (reviewed in (47)). In addition, several members of PRC1 (polycomb repressive complex 1) that recognizes H3K27 methylation (reviewed in (48)) were also identified on H3.1 nucleosomes. On the other hand, H3.Y nucleosomes contained H3.3 and showed a strong binding of the chaperone and transcriptional elongation complex FACT (facilitates chromatin transcription) members FACT80 and FACT140 (49). These data suggest that H3.1- and H3.Y-containing nucleosomes differ in their H3 variant composition and in their association with repressive and activating protein complexes (Figure 4D).

Interestingly, although both H3.3 and H3.Y were bound to HIRA in a non-chromatin context, their differential DAXX binding ability led to apparent differences in the chromatin environment detected at the nucleosomal level (Figure 4E). In a direct comparison, H3.3 nucleosomes showed an accumulation of 'writers' and 'readers' of the repressive H3K9me3 modification, while H3.Y nucleosomes still showed an enrichment of the FACT complex. Next, we tested whether differential association of SUV39H enzymes with distinct H3 variant-containing nucleosomes directly affects H3K9me3 levels *in vivo*. In agreement with our ChIP-seq data (Figure 3D–F), immunoblots of eGFP-H3 variant mononucleosome pull-downs indeed confirmed a reduction of K9me3 on endogenous H3 in H3.Y-containing nucleosomes compared to nucleosomes with other H3 variants (Figure 4F). As a consequence, H3.Y nucleosomes appear to exist as heterotypic nucleosomes containing H3.3 and to be enriched in the FACT complex, suggestive of H3.Y's involvement in transcriptional activation. These observations are consistent with H3.Y being solely deposited by HIRA into open, H3K9me3-depleted chromatin and not by DAXX/ATRX, and are in agreement with a recent study showing H3.Y localization to transcription start sites of active genes (50).

In summary, H3.Y is deposited into open euchromatic sites leading to the recruitment of FACT, while it is depleted

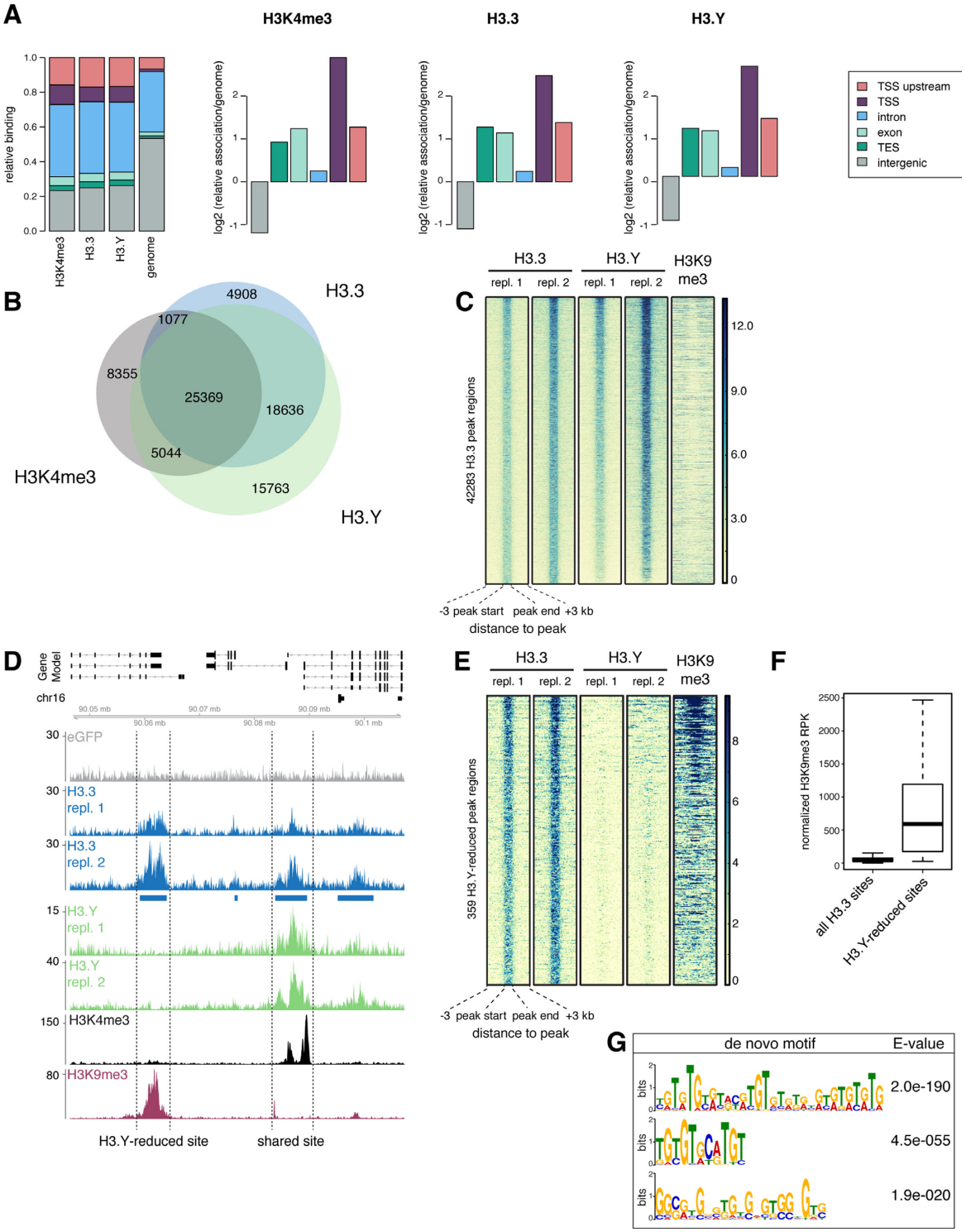

Figure 3. H3.3-containing, H3.Y-reduced sites are enriched in H3K9me3 and simple repeat sequences. (**A**) Annotation of H3.3-, H3.Y- and H3K4me3-enriched regions as determined by ChIP-seq in comparison to the total genome. Data for H3K4me3 is from ENCODE consortium. (**B**) Venn diagram of H3.3, H3.Y and H3K4me3 peaks (depicted are numbers of peaks). (**C**) ChIP-seq density heat map for peaks identified in H3.3 replicate 1 and correlated to second H3.3 replicate, as well as both H3.Y replicates and H3K9me3. Data for H3K9me3 is from (64) (GEO repository sample GSM2308949 (GSE86811)). Color intensity represents normalized and globally scaled tag counts. (**D**) Genome browser snap shot of a representative region in chromosome 16 displaying eGFP control (gray), two H3.3 replicates (blue), two H3.Y replicates (green), H3K4me3 (black) and H3K9me3 (red) ChIP-seq signals. Blue bars depict assigned peaks using MACS 2 peak calling method. Annotated gene structures are shown above. Highlighted are H3.3/H3.Y-shared (right) and H3.3-enriched, H3.Y-reduced (left) sites. (**E**) Density heat map for peaks representing H3.3-enriched, H3.Y-reduced sites correlated to H3K9me3. Color intensity represents normalized and globally scaled tag counts. (**F**) Box plot of H3K9me3 signal intensity comparing all H3.3-enriched peaks with H3.Y-reduced peaks. RPK: reads per kilobase. (**G**) *Denovo* motif search results with H3.3-containing, H3.Y-reduced sites using MEME (http://meme-suite.org/tools/meme; (65)), see also Supplementary Figure S1 for hierarchical clustering of top 50 repeat sequences.

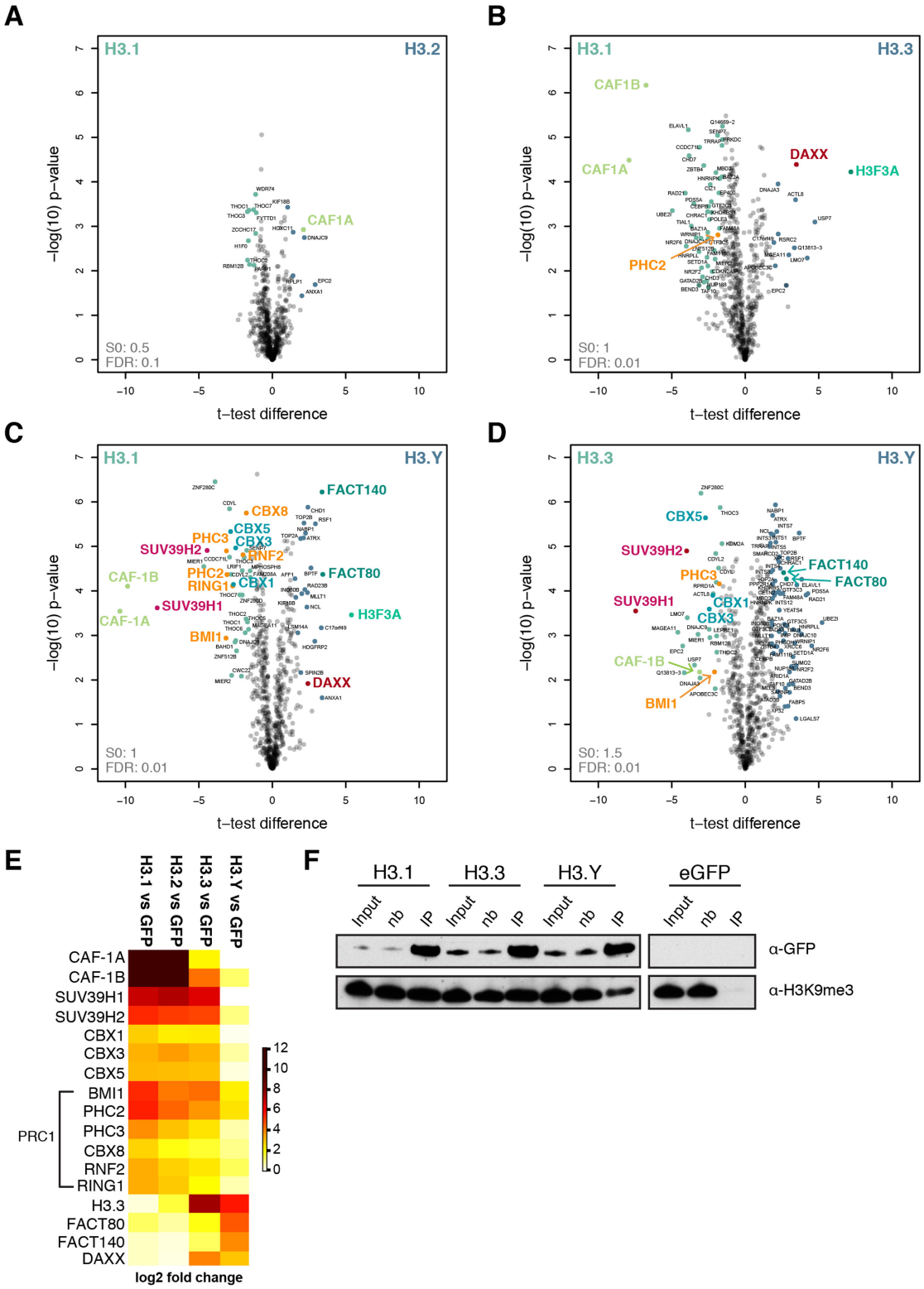

Figure 4. H3.Y-containing nucleosomes are enriched with FACT complex and reduced in repressive H3K9me3. (**A**–**D**) Identification of proteins enriched on eGFP-H3.1-, eGFP-H3.2-, eGFP-H3.3- or eGFP-H3.Y-mononucleosomes (see Supplementary Figure S2A) derived from HK cells after eGFP normalization (see Supplementary Figure S2B–D). Pull-downs of mononucleosomes containing H3.1 versus H3.2 (A), H3.1 versus H3.3 (B), H3.1 versus H3.Y (C) and H3.3 versus H3.Y (D) are displayed in volcano plots by plotting *P*-values and *t*-test differences obtained from two-sample *t*-test. Significantly enriched proteins are determined using a permutation-based FDR cutoff and labeled. All identified proteins are listed in Supplementary Tables S5–9. (**E**) Log2-fold changes of interacting proteins of mononucleosome-IPs (A–D) visualized in a heatmap. (**F**) Immunoblots of eGFP-H3 variant pulldowns using mononucleosomes derived from HK cells using α-GFP and α-H3K9me3 antibodies. nb, non-bound fraction after precipitation, IP, immunoprecipitated material.

from H3K9me3-containing heterochromatic simple repeat regions, likely due to its inability to interact with DAXX.

DAXX recognition of H3 variants depends on a combination of H3.3 core and C-terminal amino acids

Our findings indicate thus far that H3.Y associates with HIRA but not DAXX, while H3.Y's chaperone recognition site is identical to that of H3.3. Thus, we determined which residues are necessary and sufficient for the DAXX–H3.3 interaction. To this end, we used H3.Y as a 'natural' H3.3 mutant to reconstitute DAXX interaction in a 'gain-of-function' mutational screen. This has the benefit of identifying all amino acids sufficient for chaperone recognition. Therefore, we exchanged unique H3.Y residues with H3.3 amino acids and tested which mutants would be able to bind DAXX. Hence, we generated HK stable cell lines expressing eGFP-H3.Y mutants, verified their expression levels by flow cytometry, tested for their correct nuclear localization and stable chromatin incorporation by immunofluorescence (IF) microscopy and performed pull-down and PML-NB recruitment assays.

First, we mutated H3.Y's unique glutamine to H3.3's glutamic acid at position 59 (H3.YQ59E) (Figure 5A, top). We chose this particular residue, as published crystal structures of the DAXX–H3.3-H4 complex demonstrated that the side chains of Q59 together with S57 (present in both H3.3 and H3.Y) participate in a hydrogen bonding network with several DAXX residues (51,52). Additionally, one of these studies also showed that depletion of residues 1–60 of H3.3, but not of 1–43 abrogated DAXX binding (51), suggesting a strong impact of residues 44–60 on histone H3.3 association. Remarkably, exchanging glutamine to glutamic acid in H3.Y at position 59 did not establish efficient DAXX binding as judged from pull-down assays from chromatin-free nuclear extracts (Figure 5A, bottom and Supplementary Figure S3). Next, we investigated whether amino acid differences adjacent to the chaperone recognition site (87–90) might influence DAXX interaction. A region spanning from residues 77 to 80 varies completely between H3.Y and H3.3 (Figure 5A, top); thus we speculated that this stretch might have structural implications for the protein region containing the chaperone recognition site. We therefore exchanged all five different amino acids to match the H3.3 sequence in the background of the eGFP-H3.YQ59E mutant. This triple core region mutant (eGFP-H3.Y Q59E A77D I78F S79K P80T Q102G; in short, 'H3.Y core') retained the ability to assemble into chromatin (Supplementary Figure S4); however, it did not gain DAXX binding ability (Figure 5A, bottom). Thus, we conclude that core amino acids directly surrounding the chaperone recognition site and participating in DAXX association (51,52) are not sufficient for a strong DAXX–H3 interaction.

We then generated different 'tail-swap' mutants, as a strategy to assess whether N- or C-terminal amino acids are necessary for DAXX binding (Figure 5B, top and Supplementary Figure S5):

i. H3.Y with an N-terminus derived from H3.3 (N3-Y), to determine whether N-terminal amino acids or specific PTMs therein (such as H3K14ac, a deposition mark in lower eukaryotes (53)) are needed for DAXX binding in combination with the conserved chaperone recognition site;
ii. H3.3 with the unique H3.Y N-terminus (NY-3), to determine whether H3.Y-specific N-terminal residues or PTMs might prevent DAXX association;
iii. H3.3 N-terminus and core with the C-terminus of H3.Y (3-CY), to assess any involvement of C-terminal residues, as recently proposed (54);
iv. lastly, H3.Y with the H3.3 C-terminal tail (Y-C3), to determine whether the H3.3 C-terminal tail suffices for DAXX binding.

Interestingly, only NY-3, albeit none of the other histone chimeras, was able to restore DAXX binding (Figure 5B, bottom). Functionally, this chimera was efficiently targeted to PML bodies (Figure 5C), verifying the gain of DAXX-interaction ability. Surprisingly, we also observed PML body recruitment of the 3-CY mutant that did not show any DAXX interactions in biochemical assays (Figure 5C). This raises the possibility that this mutant only transiently, but functionally, binds DAXX or that an additional currently unidentified DAXX-independent pathway for PML body recruitment exists.

Concluding, these data suggest that H3.3's N-terminus till amino acid 35 is not required for DAXX binding and PML-NB recruitment. However, H3.3's core region alone is not sufficient for the establishment of a strong DAXX interaction but enables PML-NB localization.

Therefore, we first dissected the role of H3.3 C-terminal tail amino acids in PML-NB recruitment by generating mutants of this region in the H3.Y core background sequence (Figure 6A, top and Supplementary Figure S6). While, as expected, none of the mutants were able to efficiently pull-down DAXX (Figure 6A, bottom), additional exchange of H3.Y's lysine 53 to arginine in combination with R122K and M124I mutations (K53R R122K M124I) enabled PML-NB localization (Figure 6B). In agreement with this data, substitution of the complete C-terminus in the K53R core background (K53R C3) also fostered PML-NB recruitment. Surprisingly, replacement of the last three amino acids (K53R GERA; GERA) did not facilitate PML-NB enrichment, suggesting that some few specific amino acids determine cellular localization of H3 histones.

Next, we determined which core amino acids are responsible for a strong DAXX interaction (Figure 6C, top, Supplementary Figure S7), or phrased differently, prevent DAXX association. We introduced point mutations into the H3.Y K53R core C3 background sequence, as it enabled PML-NB localization and did only differ in three amino acids from the core region in H3.3. Therefore, H3.Y's unique K42, L46 and L62, either alone or in combinations, seem to be responsible for its inability to strongly bind DAXX. Interestingly, the exchange of leucine 46 to valine (L46V) and to a minor extent, of K42R but not of L62I, resulted in a detectable DAXX interaction (Figure 6C, bottom). Similarly, both double exchange combinations containing the L46V mutation (K42R L46V and L46V L62I) showed increased DAXX interaction.

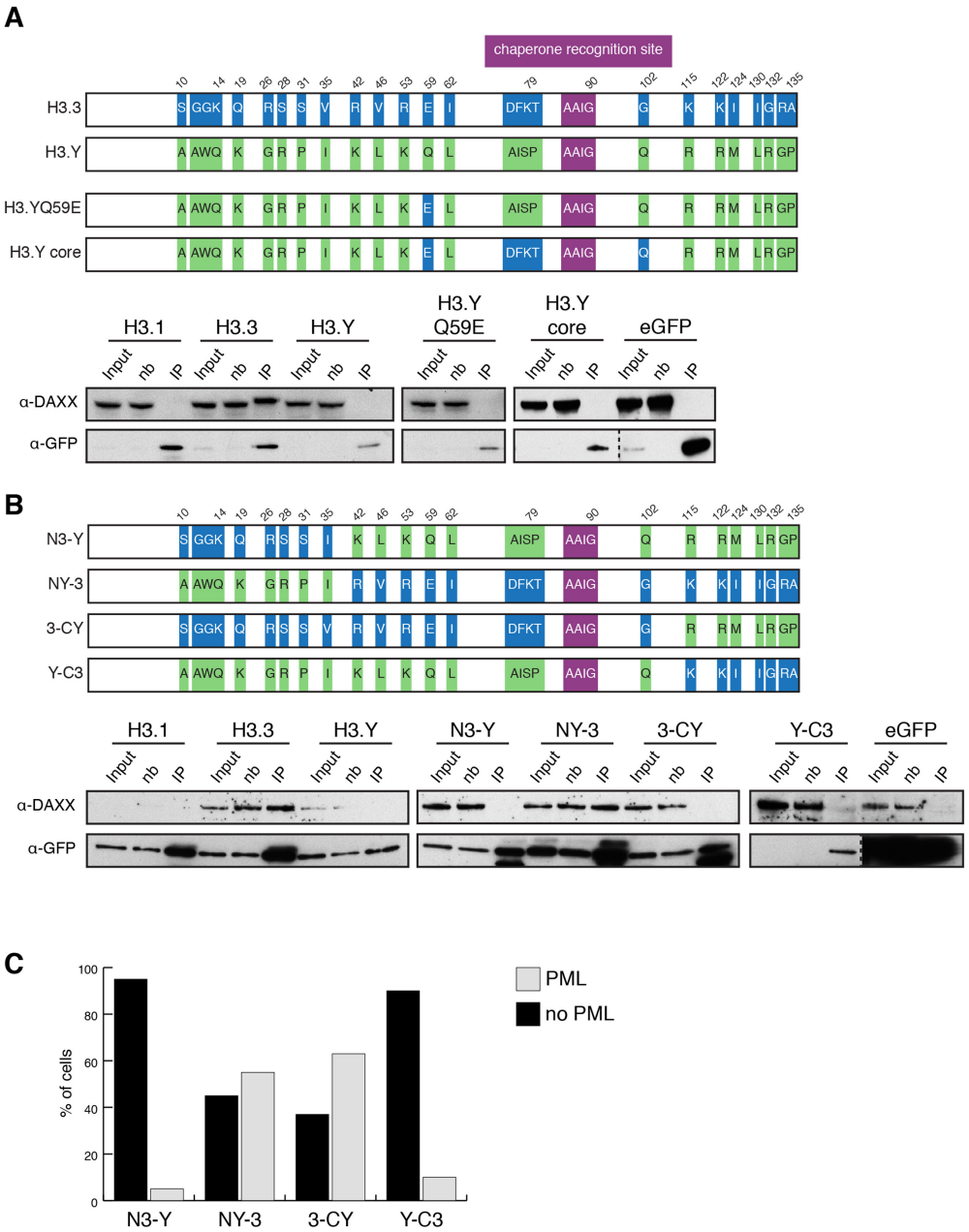

Figure 5. H3.3 core region in combination with C-terminal sequence is sufficient for DAXX interaction. (**A** and **B**) Top: schematical alignment of H3.3, H3.Y and H3.Y core (A) and H3.3/H3.Y 'tail-swap' (B) mutant proteins. H3.3-specific amino acids are highlighted in blue, whereas H3.Y-unique residues are depicted in green boxes. Shared chaperone recognition sequence is shown in purple. Bottom: soluble nuclear extracts from HK cells stably expressing eGFP-tagged H3 variants as well as H3.YQ59E and H3.Y core (A) or H3.Y/H3.3 'tail-swap' mutants (B) were used for pull-down experiments as described in Figure 2A. One out of at least two representative immunoblots is shown. Proper nuclear and chromatin localization of all eGFP-H3 variants and H3.Y core mutants is shown in Supplementary Figures S3 and 4 and of chimeric constructs in Supplementary Figure S5A and B. (**C**) Quantification of 200 cells 24 h after transfection (see Supplementary Figure S5C for IF analysis) showing the localization of different eGFP-H3.3/H3.Y 'tail-swap' mutants to PML-NBs (gray) or not (black).

In summary, these data imply that strong DAXX binding is prevented when H3.3's amino acid at position 46 is mutated to H3.Y's unique leucine residue.

DAXX interaction is required to induce H3 variant deposition at heterochromatic H3K9me3-enriched simple repeats

Next, we wondered whether gain of DAXX binding would also enable H3.Y mutants to be deposited into heterochromatic H3.Y-reduced sites. We therefore chose to determine regions of chromatin incorporation by ChIP-seq of all 'tail-swap' chimeras and the gain-of-function L46V L62I mu-

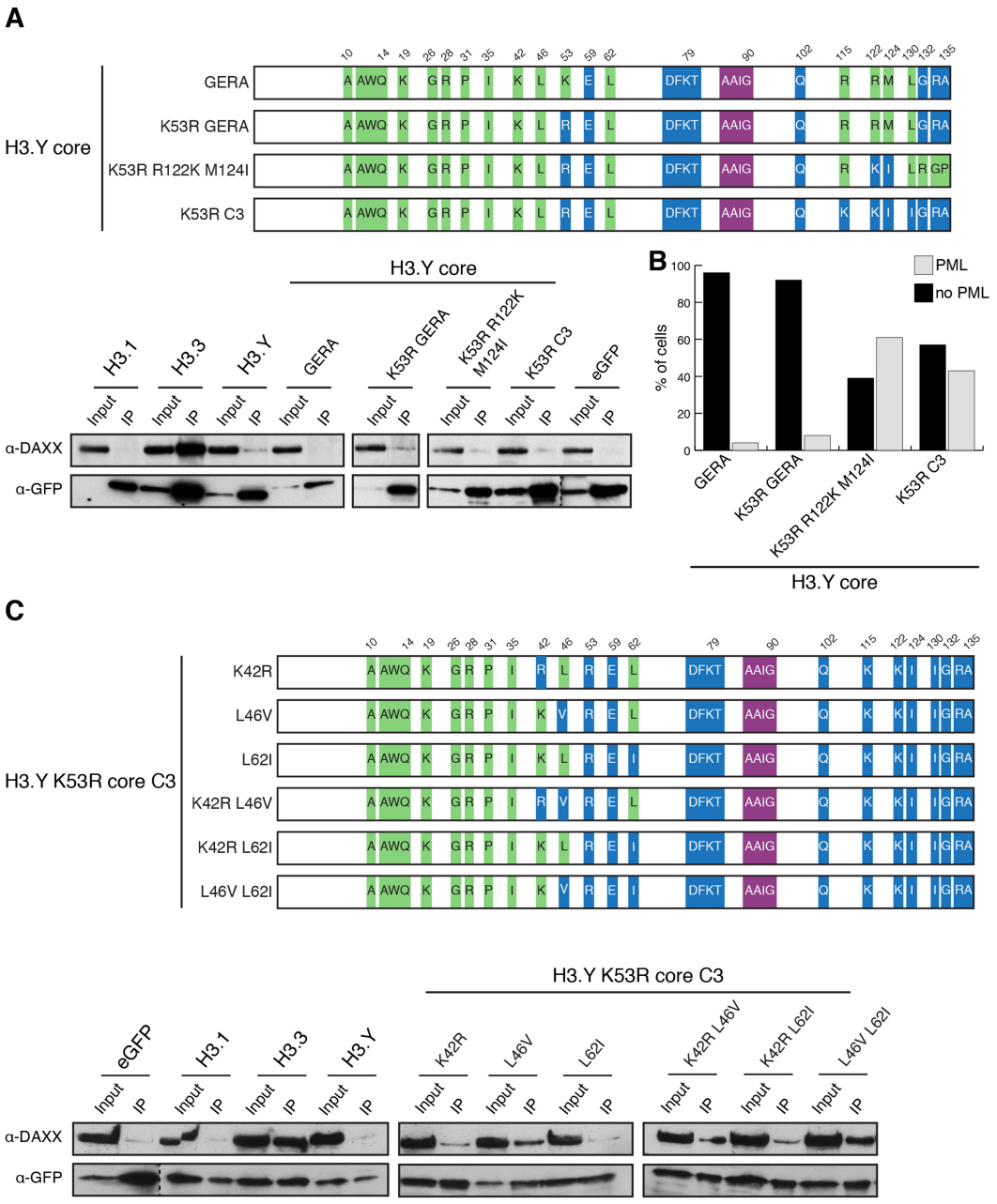

Figure 6. DAXX interaction is repelled by H3.Y's unique leucine at position 46. (**A** and **C**) Top: schematical alignment as seen in Figure 5A and B showing H3.Y C-terminal tail (A) or H3.3 core (C) mutant proteins. Bottom: soluble nuclear extracts from HK cells stably expressing eGFP-tagged H3.Y C-terminal tail (A) or H3.3 core (C) mutants were used for pull-down experiments as described in Figure 2A. One of at least two representative immunoblots is shown. Expression levels and proper nuclear and chromatin localization of all eGFP-H3.Y C-terminal mutants is shown in Supplementary Figure S6 and of H3.3 core mutants constructs in Supplementary Figure S7. (**B**) PML-NB localization quantification of different eGFP-H3.3 core mutants as described in Figure 5C.

tant. As expected, all mutants, regardless of their DAXX-binding ability, were deposited into chromatin sites that showed both H3.3 and H3.Y enrichment (Figure 7A). To investigate whether the gain of DAXX binding changed their deposition pattern, we further analyzed regions characterized by the presence of H3.3 and absence of H3.Y (see Figure 4D). Strikingly, those mutants that gained DAXX-binding ability (NY-3 and L46V L62I) were now present at many H3.Y-reduced regions, while mutants that neither bind DAXX nor localize to PML-NBs (Y-C3, N3-Y) remained depleted from these regions (Figure 7B and C; Supplementary Table S10 for statistical evaluation). Interestingly, the 3-CY mutant able to localize to PML-NB without showing a strong DAXX interaction (see Figure 5B and C) showed an intermediate phenotype. It was slightly enriched at some but not at all H3.Y-reduced sites (Figure 7B and C; Supplementary Table S10). These data sets suggest that DAXX binding is necessary and sufficient for histone H3

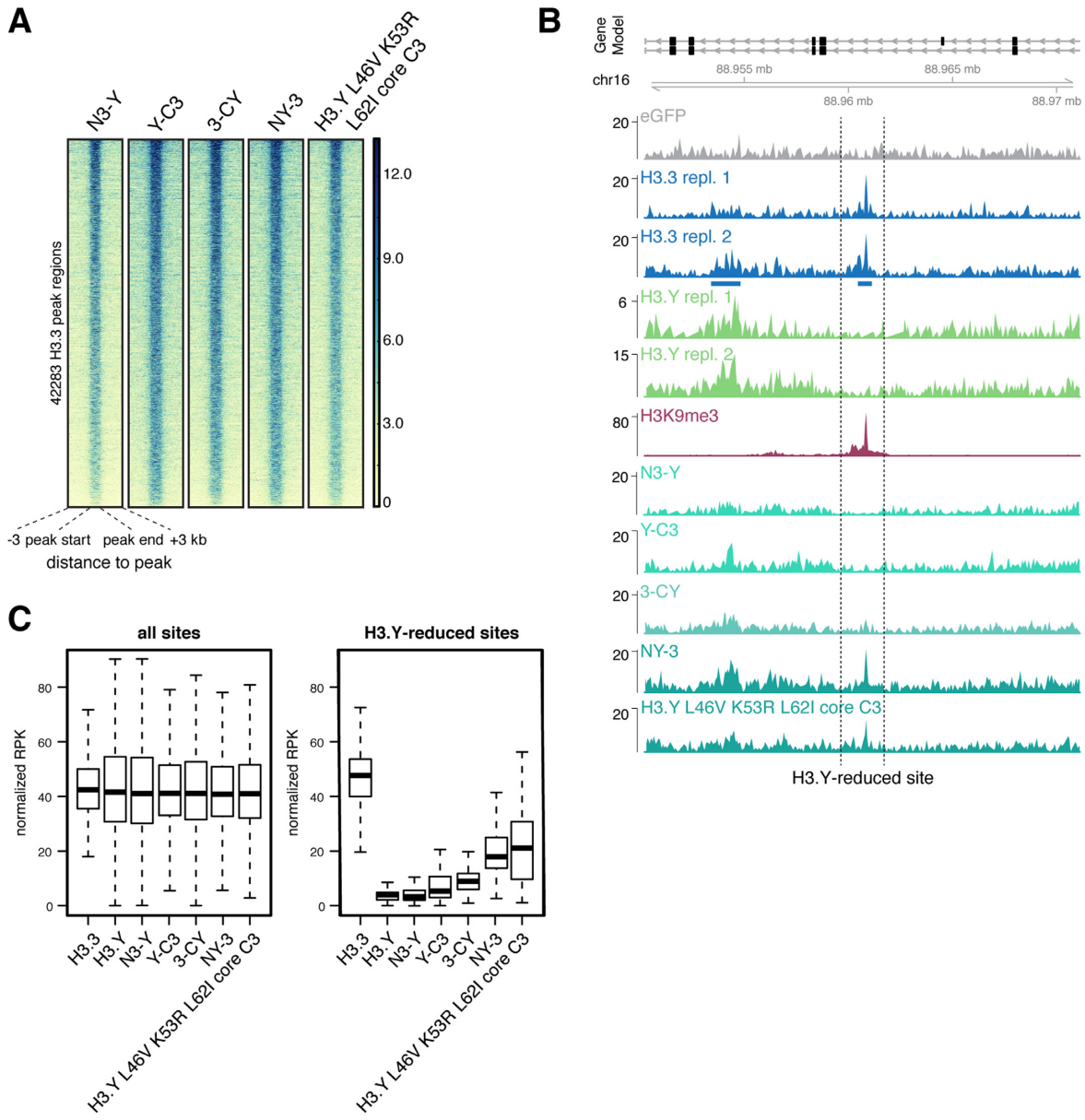

Figure 7. Restoration of DAXX binding to H3.Y mutants enables deposition at heterochromatin sites. (**A**) ChIP-seq density heat map of H3.3 as described in Figure 3C listing H3.3/H3.Y 'tail-swap' and H3.Y L46V K53R L62I core C3 mutant signals. Data for H3K9me3 is from (64) (GEO repository sample GSM2308949 (GSE86811)). Color intensity represents normalized and globally scaled tag counts. (**B**) Genome browser snap shot of representative region displaying 'tail-swap' and H3.Y L46V K53R L62I core C3 mutant protein (turquoise) ChIP-seq signals at H3.3-enriched, H3.Y-reduced heterochromatin sites (see Figure 3D). (**C**) Box plot of peak signal intensities of H3.3/H3.Y 'tail-swap' and H3.Y L46V K53R L62I core C3 mutant signals comparing all H3.3-enriched sites with H3.Y-reduced sites. Shown are mean signal intensities of two H3.3 and H3.Y replicates. Testing for statistical significance of observed differences was done using Wilcoxon-signed-rank test (Supplementary Table S10).

deposition in human H3K9me3 heterochromatic sites and that PML-NB localization enables deposition to some but not all DAXX-dependent regions.

DISCUSSION

We have identified the human chaperone/remodeling and mononucleosome binding complexes of the primate-specific histone variant H3.Y. We show that H3.Y interacts with members of the HIRA complex, but not DAXX/ATRX, due to some H3.Y's unique core and C-terminal amino acids. Accordingly, H3.Y is incorporated into genic regions that are enriched with H3K4me3 and depleted from DAXX/ATRX-target sites characterized by H3K9me3 and simple repeat enrichment. In concordance, H3.Y-containing nucleosomes are associated with factors involved in transcription. These data are entirely consistent with our previous findings of H3.Y being a histone variant involved in gene activation (7).

The HIRA (or HUCA) complex is responsible for enrichment of H3.3 in the body of expressed genes and at promoters of transcribed and non-transcribed genes (55). Additionally, transiently accessible non-nucleosomal DNA generated as a result of transcription or remodeling is a target for H3.3 deposition by HIRA in a so-called 'gap-filling mechanism' (42,43). In agreement with an HIRA-dependent and DAXX-independent deposition mechanism, H3.Y accumulates at open H3K4me3-marked genic regions and is depleted from H3K9me3 heterochromatic sites. Interestingly, while genomic DAXX/ATRX-target regions in mouse ESCs include telomeric repeats, endogenous retroviral elements, imprinted differentially methylated regions and selected intragenic methylated CpG islands (56), we found an enrichment of simple repeats in humans. While H3.3 deposition into repeat families is common in both organisms, it still needs to be determined whether the discrepancy in the nature of such elements is due to experimental or technical limitations, such as cross-linking and shearing differences, or indeed originates from a biological cause.

Further confirmation of H3.Y being correlated with open chromatin was seen in the enrichment of the FACT complex on H3.Y-containing mononucleosomes. FACT reorganizes nucleosomes through the disruption of core histone-histone and histone-DNA interactions and regulates transcription, replication and DNA repair processes (57). It is therefore tempting to speculate that newly synthesized H3.Y is deposited into euchromatic regions by HIRA, and FACT may help H3.Y incorporation into active regions depleted of nucleosomes upon RNA Polymerase II transit. If true, heterotypic mononucleosomes containing both H3.3 and H3.Y should exist. Our findings and recent results (50) support this view. Indeed, we identify H3.3 in a complex with eGFP-H3.Y-containing nucleosomes. Moreover, *in vitro* biochemical reconstitution assays show that H3.Y/H3.3 heterotypic nucleosomes can be formed, and that these are more susceptible to MNase digestion than H3.3 homotypic nucleosomes (50). In addition, we note a depletion of H3K9me3, SUV39H1/2, HP1 isoforms and PRC1 members from H3.Y nucleosomes, highly consistent with incorporation of H3.Y into transcriptionally active, H3K9me3-depleted regions.

Most significantly, we find that DAXX and HIRA, which were thought to share the identical interaction region in H3.3 (55), appear to have distinct requirements for histone variant recognition. H3.Y contains the chaperone recognition site of H3.3, yet is unable to bind DAXX/ATRX. Thus, H3.Y represents the perfect endogenous 'mutant' to biochemically dissect the distinct histone binding requirements of DAXX. H3.3 and H3.Y differ in 26 amino acids with only 9 being similar replacements. Still, both variants contain the identical chaperone recognition site in their α2 helix spanning amino acids 87–90, which allows a functional distinction between H3.3- and H3.1/H3.2-specific chaperone/remodeler interactions (51,52). Employing a gain-of-function screen to identify those amino acids in H3.3 required for DAXX binding or, in turn, mediating DAXX repulsion in the case of H3.Y, we were able to separate DAXX binding from PML-NB localization sequence requirements (summarized in Supplementary Figure S8). Our tail-swap mutation approach shows that the N-terminal tail of H3.3 is neither needed for DAXX interaction, which is in agreement with *in vitro* data (51), nor for PML-NB localization. This result is supported by a recent hydrogen/deuterium exchange MS study that proposes a stepwise scanning and folding pathway to explain the fidelity of DAXX-H3.3 binding (54). However, our step-by-step gain-of-function screen revealed the importance of H3.3's arginine 53, lysine 122 and isoleucine 124 for PML-NB localization, while being insufficient for strong DAXX binding. Then again, biochemically visible DAXX interaction was only observed when also a valine was present at position 46 instead of a leucine. These observations open up interesting possibilities regarding the proposed functional requirement of DAXX binding for PML-NB recruitment (20). While it is possible that even a DAXX-independent PML-NB localization mechanism of H3 variants exist, our tail-swap ChIP-seq data argue against it. Considering the fact that 3-CY is slightly enriched at some H3.Y-reduced sites, we speculate that it is able to interact with DAXX, albeit with low affinity and only transiently. This would still allow PML-NB localization and DAXX/ATRX-mediated deposition to some genomic target sites that probably show the highest recruitment affinity. If true, it will be of interest to find out whether and which DNA sequence and/or chromatin features determine DAXX/ATRX recognition and binding strength.

Further, are structural aspects and/or PTMs of or in the vicinity of H3.3's valine 46, arginine 53, lysine 122 and isoleucine 124 responsible for DAXX interaction? So far, most of closed-by modified residues have been correlated to transcriptional activation (in the case of Y41 phosphorylation and acetylation of K122 (58,59)), or DNA damage repair (T45 phosphorylation (60)). Yet, it is rather unlikely that these PTMs are functionally connected to DAXX binding and H3.3 deposition at heterochromatin sites. This is reinforced by recent studies in mESCs and mouse embryonic fibroblasts suggesting that DAXX/ATRX-dependent deposition is important for maintaining heterochromatin (61) by repressing transcription (62).

In conclusion, our study has revealed surprising new insights into H3.Y deposition mechanisms, as well as DAXX-histone H3 interaction necessities and human DAXX/ATRX chromatin targeting requirements.

PRIMARY ACCESSIONS

The data discussed in this publication has been deposited in NCBI's Gene Expression Omnibus (63). ChIP-seq data have been uploaded to NCBI under GEO accession number GSE94034.

SUPPLEMENTARY DATA

Supplementary Data are available at NAR Online.

ACKNOWLEDGEMENTS

We would like to thank Antonia Jack for discussions and Silvia Härtel for experimental support. Many thanks to Filippo Cernilogar (LMU Munich) for providing his ChIP-seq

protocol and to Stefan Krebs from LAFUGA (Gene Center Munich) for help and advice in high-throughput sequencing. L.M.Z. carried out all FACS analyses, IF nuclear staining and microscopy and DAXX interaction studies, H.C.E. performed SILAC pull-downs and MS analyses, E.C.K. acquired and analyzed label-free quantitative MS data, S.P. generated eGFP-H3.YQ59E mutant construct and cell line, C.B. cloned eGFP-H3 variant plasmids and generated the respective stable cell lines, E.D. investigated PML body co-localizations, M.B. performed all bioinformatic analyses of ChIP-seq data, P.C., M.M. and S.B.H participated in the experimental design and interpretation of the data and S.B.H. conceived the study, participated in its design and wrote the manuscript. All authors read and approved of the final manuscript.

FUNDING

German Research Foundation (DFG) [SFB/TR5, project M10; SFB1064, project A10] (to S.B.H); Center for Integrated Protein Science Munich (CIPSM) (to S.B.H., M.M); TRR81 of the DFG (to M.B.); Norwegian Cancer Society (to E.D.); Research Council of Norway (to P.C.). Funding for open access charge: DFG.
Conflict of interest statement. None declared.

REFERENCES

1. van Holde,K.E. (1988) *Chromatin*. Springer, NY.
2. Luger,K., Mader,A.W., Richmond,R.K., Sargent,D.F. and Richmond,T.J. (1997) Crystal structure of the nucleosome core particle at 2.8 A resolution. *Nature*, **389**, 251–260.
3. Bonisch,C., Nieratschker,S.M., Orfanos,N.K. and Hake,S.B. (2008) Chromatin proteomics and epigenetic regulatory circuits. *Expert Rev. Proteomics*, **5**, 105–119.
4. Burgess,R.J. and Zhang,Z. (2013) Histone chaperones in nucleosome assembly and human disease. *Nat. Struct. Mol. Biol.*, **20**, 14–22.
5. Hake,S.B., Garcia,B.A., Duncan,E.M., Kauer,M., Dellaire,G., Shabanowitz,J., Bazett-Jones,D.P., Allis,C.D. and Hunt,D.F. (2006) Expression patterns and post-translational modifications associated with mammalian histone H3 variants. *J. Biol. Chem.*, **281**, 559–568.
6. Hake,S.B. and Allis,C.D. (2006) Histone H3 variants and their potential role in indexing mammalian genomes: the "H3 barcode hypothesis". *Proc. Natl. Acad. Sci. U.S.A.*, **103**, 6428–6435.
7. Wiedemann,S.M., Mildner,S.N., Bonisch,C., Israel,L., Maiser,A., Matheisl,S., Straub,T., Merkl,R., Leonhardt,H., Kremmer,E. *et al.* (2010) Identification and characterization of two novel primate-specific histone H3 variants, H3.X and H3.Y. *J. Cell Biol.*, **190**, 777–791.
8. Talbert,P.B., Ahmad,K., Almouzni,G., Ausio,J., Berger,F., Bhalla,P.L., Bonner,W.M., Cande,W.Z., Chadwick,B.P., Chan,S.W. *et al.* (2012) A unified phylogeny-based nomenclature for histone variants. *Epigenet. Chromatin*, **5**, 7.
9. Ransom,M., Dennehey,B.K. and Tyler,J.K. (2010) Chaperoning histones during DNA replication and repair. *Cell*, **140**, 183–195.
10. Mattiroli,F., D'Arcy,S. and Luger,K. (2015) The right place at the right time: chaperoning core histone variants. *EMBO Rep.*, **16**, 1454–1466.
11. Tagami,H., Ray-Gallet,D., Almouzni,G. and Nakatani,Y. (2004) Histone H3.1 and H3.3 complexes mediate nucleosome assembly pathways dependent or independent of DNA synthesis. *Cell*, **116**, 51–61.
12. Tang,Y., Puri,A., Ricketts,M.D., Rai,T.S., Hoffmann,J., Hoi,E., Adams,P.D., Schultz,D.C. and Marmorstein,R. (2012) Identification of an ubinuclein 1 region required for stability and function of the human HIRA/UBN1/CABIN1/ASF1a histone H3.3 chaperone complex. *Biochemistry*, **51**, 2366–2377.
13. Li,X. and Tyler,J.K. (2016) Nucleosome disassembly during human non-homologous end joining followed by concerted HIRA- and CAF-1-dependent reassembly. *Elife*, **5**, e15129.
14. Goldberg,A.D., Banaszynski,L.A., Noh,K.M., Lewis,P.W., Elsaesser,S.J., Stadler,S., Dewell,S., Law,M., Guo,X., Li,X. *et al.* (2010) Distinct factors control histone variant H3.3 localization at specific genomic regions. *Cell*, **140**, 678–691.
15. Wong,L.H., McGhie,J.D., Sim,M., Anderson,M.A., Ahn,S., Hannan,R.D., George,A.J., Morgan,K.A., Mann,J.R. and Choo,K.H. (2010) ATRX interacts with H3.3 in maintaining telomere structural integrity in pluripotent embryonic stem cells. *Genome Res.*, **20**, 351–360.
16. Drane,P., Ouararhni,K., Depaux,A., Shuaib,M. and Hamiche,A. (2010) The death-associated protein DAXX is a novel histone chaperone involved in the replication-independent deposition of H3.3. *Genes Dev.*, **24**, 1253–1265.
17. Wong,L.H., Ren,H., Williams,E., McGhie,J., Ahn,S., Sim,M., Tam,A., Earle,E., Anderson,M.A., Mann,J. *et al.* (2009) Histone H3.3 incorporation provides a unique and functionally essential telomeric chromatin in embryonic stem cells. *Genome Res.*, **19**, 404–414.
18. Zink,L.M. and Hake,S.B. (2016) Histone variants: nuclear function and disease. *Curr. Opin. Genet. Dev.*, **37**, 82–89.
19. Bonisch,C., Schneider,K., Punzeler,S., Wiedemann,S.M., Bielmeier,C., Bocola,M., Eberl,H.C., Kuegel,W., Neumann,J., Kremmer,E. *et al.* (2012) H2A.Z.2.2 is an alternatively spliced histone H2A.Z variant that causes severe nucleosome destabilization. *Nucleic Acids Res.*, **40**, 5951–5964.
20. Delbarre,E., Ivanauskiene,K., Kuntziger,T. and Collas,P. (2013) DAXX-dependent supply of soluble (H3.3-H4) dimers to PML bodies pending deposition into chromatin. *Genome Res.*, **23**, 440–451.
21. Vermeulen,M., Eberl,H.C., Matarese,F., Marks,H., Denissov,S., Butter,F., Lee,K.K., Olsen,J.V., Hyman,A.A., Stunnenberg,H.G. *et al.* (2010) Quantitative interaction proteomics and genome-wide profiling of epigenetic histone marks and their readers. *Cell*, **142**, 967–980.
22. Vermeulen,M., Mulder,K.W., Denissov,S., Pijnappel,W.W., van Schaik,F.M., Varier,R.A., Baltissen,M.P., Stunnenberg,H.G., Mann,M. and Timmers,H.T. (2007) Selective anchoring of TFIID to nucleosomes by trimethylation of histone H3 lysine 4. *Cell*, **131**, 58–69.
23. Sansoni,V., Casas-Delucchi,C.S., Rajan,M., Schmidt,A., Bonisch,C., Thomae,A.W., Staege,M.S., Hake,S.B., Cardoso,M.C. and Imhof,A. (2014) The histone variant H2A.Bbd is enriched at sites of DNA synthesis. *Nucleic Acids Res.*, **42**, 6405–6420.
24. Vardabasso,C., Gaspar-Maia,A., Hasson,D., Punzeler,S., Valle-Garcia,D., Straub,T., Keilhauer,E.C., Strub,T., Dong,J., Panda,T. *et al.* (2015) Histone variant H2A.Z.2 mediates proliferation and drug sensitivity of malignant melanoma. *Mol. Cell*, **59**, 75–88.
25. Rappsilber,J., Mann,M. and Ishihama,Y. (2007) Protocol for micro-purification, enrichment, pre-fractionation and storage of peptides for proteomics using StageTips. *Nat. Protoc.*, **2**, 1896–1906.
26. Cox,J. and Mann,M. (2008) MaxQuant enables high peptide identification rates, individualized p.p.b.-range mass accuracies and proteome-wide protein quantification. *Nat. Biotechnol.*, **26**, 1367–1372.
27. Tyanova,S., Temu,T., Sinitcyn,P., Carlson,A., Hein,M.Y., Geiger,T., Mann,M. and Cox,J. (2016) The Perseus computational platform for comprehensive analysis of (prote)omics data. *Nat. Methods*, **13**, 731–740.
28. Keilhauer,E.C., Hein,M.Y. and Mann,M. (2015) Accurate protein complex retrieval by affinity enrichment mass spectrometry (AE-MS) rather than affinity purification mass spectrometry (AP-MS). *Mol. Cell. Proteomics*, **14**, 120–135.
29. Hake,S.B., Garcia,B.A., Kauer,M., Baker,S.P., Shabanowitz,J., Hunt,D.F. and Allis,C.D. (2005) Serine 31 phosphorylation of histone variant H3.3 is specific to regions bordering centromeres in metaphase chromosomes. *Proc. Natl. Acad. Sci. U.S.A.*, **102**, 6344–6349.
30. Langmead,B. and Salzberg,S.L. (2012) Fast gapped-read alignment with Bowtie 2. *Nat. Methods*, **9**, 357–359.
31. Bulut-Karslioglu,A., De La Rosa-Velazquez,I.A., Ramirez,F., Barenboim,M., Onishi-Seebacher,M., Arand,J., Galan,C., Winter,G.E., Engist,B., Gerle,B. *et al.* (2014) Suv39h-dependent

H3K9me3 marks intact retrotransposons and silences LINE elements in mouse embryonic stem cells. *Mol. Cell*, **55**, 277–290.
32. Feng,J., Liu,T., Qin,B., Zhang,Y. and Liu,X.S. (2012) Identifying ChIP-seq enrichment using MACS. *Nat. Protoc.*, **7**, 1728–1740.
33. Gentleman,R.C., Carey,V.J., Bates,D.M., Bolstad,B., Dettling,M., Dudoit,S., Ellis,B., Gautier,L., Ge,Y., Gentry,J. *et al.* (2004) Bioconductor: open software development for computational biology and bioinformatics. *Genome Biol.*, **5**, R80.
34. Love,M.I., Huber,W. and Anders,S. (2014) Moderated estimation of fold change and dispersion for RNA-seq data with DESeq2. *Genome Biol.*, **15**, 550.
35. Machanick,P. and Bailey,T.L. (2011) MEME-ChIP: motif analysis of large DNA datasets. *Bioinformatics*, **27**, 1696–1697.
36. Ramirez,F., Dundar,F., Diehl,S., Gruning,B.A. and Manke,T. (2014) deepTools: a flexible platform for exploring deep-sequencing data. *Nucleic Acids Res.*, **42**, W187–W191.
37. Hahne,F. and Ivanek,R. (2016) Visualizing genomic data using gviz and bioconductor. *Methods Mol. Biol.*, **1418**, 335–351.
38. Galvani,A., Courbeyrette,R., Agez,M., Ochsenbein,F., Mann,C. and Thuret,J.Y. (2008) In vivo study of the nucleosome assembly functions of ASF1 histone chaperones in human cells. *Mol. Cell. Biol.*, **28**, 3672–3685.
39. Costa,A. and Onesti,S. (2008) The MCM complex: (just) a replicative helicase? *Biochem. Soc. Trans.*, **36**, 136–140.
40. Latreille,D., Bluy,L., Benkirane,M. and Kiernan,R.E. (2014) Identification of histone 3 variant 2 interacting factors. *Nucleic Acids Res.*, **42**, 3542–3550.
41. Ricketts,M.D., Frederick,B., Hoff,H., Tang,Y., Schultz,D.C., Singh Rai,T., Grazia Vizioli,M., Adams,P.D. and Marmorstein,R. (2015) Ubinuclein-1 confers histone H3.3-specific-binding by the HIRA histone chaperone complex. *Nat. Commun.*, **6**, 7711.
42. Ray-Gallet,D., Woolfe,A., Vassias,I., Pellentz,C., Lacoste,N., Puri,A., Schultz,D.C., Pchelintsev,N.A., Adams,P.D., Jansen,L.E. *et al.* (2011) Dynamics of histone H3 deposition in vivo reveal a nucleosome gap-filling mechanism for H3.3 to maintain chromatin integrity. *Mol. Cell*, **44**, 928–941.
43. Schneiderman,J.I., Orsi,G.A., Hughes,K.T., Loppin,B. and Ahmad,K. (2012) Nucleosome-depleted chromatin gaps recruit assembly factors for the H3.3 histone variant. *Proc. Natl. Acad. Sci. U.S.A.*, **109**, 19721–19726.
44. Elsasser,S.J., Noh,K.M., Diaz,N., Allis,C.D. and Banaszynski,L.A. (2015) Histone H3.3 is required for endogenous retroviral element silencing in embryonic stem cells. *Nature*, **522**, 240–244.
45. Lewis,P.W., Elsaesser,S.J., Noh,K.M., Stadler,S.C. and Allis,C.D. (2010) Daxx is an H3.3-specific histone chaperone and cooperates with ATRX in replication-independent chromatin assembly at telomeres. *Proc. Natl. Acad. Sci. U.S.A.*, **107**, 14075–14080.
46. Schotta,G., Ebert,A. and Reuter,G. (2003) SU(VAR)3-9 is a conserved key function in heterochromatic gene silencing. *Genetica*, **117**, 149–158.
47. Canzio,D., Larson,A. and Narlikar,G.J. (2014) Mechanisms of functional promiscuity by HP1 proteins. *Trends Cell Biol.*, **24**, 377–386.
48. Gil,J. and O'Loghlen,A. (2014) PRC1 complex diversity: where is it taking us? *Trends Cell Biol.*, **24**, 632–641.
49. Formosa,T. (2013) The role of FACT in making and breaking nucleosomes. *Biochim. Biophys. Acta*, **1819**, 247–255.
50. Kujirai,T., Horikoshi,N., Sato,K., Maehara,K., Machida,S., Osakabe,A., Kimura,H., Ohkawa,Y. and Kurumizaka,H. (2016) Structure and function of human histone H3.Y nucleosome. *Nucleic Acids Res.*, **44**, 6127–6141.
51. Elsasser,S.J., Huang,H., Lewis,P.W., Chin,J.W., Allis,C.D. and Patel,D.J. (2012) DAXX envelops a histone H3.3-H4 dimer for H3.3-specific recognition. *Nature*, **491**, 560–565.
52. Liu,C.P., Xiong,C., Wang,M., Yu,Z., Yang,N., Chen,P., Zhang,Z., Li,G. and Xu,R.M. (2012) Structure of the variant histone H3.3-H4 heterodimer in complex with its chaperone DAXX. *Nat. Struct. Mol. Biol.*, **19**, 1287–1292.
53. Sobel,R.E., Cook,R.G., Perry,C.A., Annunziato,A.T. and Allis,C.D. (1995) Conservation of deposition-related acetylation sites in newly synthesized histones H3 and H4. *Proc. Natl. Acad. Sci. U.S.A.*, **92**, 1237–1241.
54. DeNizio,J.E., Elsasser,S.J. and Black,B.E. (2014) DAXX co-folds with H3.3/H4 using high local stability conferred by the H3.3 variant recognition residues. *Nucleic Acids Res.*, **42**, 4318–4331.
55. Filipescu,D., Szenker,E. and Almouzni,G. (2013) Developmental roles of histone H3 variants and their chaperones. *Trends Genet.*, **29**, 630–640.
56. Voon,H.P. and Wong,L.H. (2016) New players in heterochromatin silencing: histone variant H3.3 and the ATRX/DAXX chaperone. *Nucleic Acids Res.*, **44**, 1496–1501.
57. Winkler,D.D. and Luger,K. (2011) The histone chaperone FACT: structural insights and mechanisms for nucleosome reorganization. *J. Biol. Chem.*, **286**, 18369–18374.
58. Dawson,M.A., Foster,S.D., Bannister,A.J., Robson,S.C., Hannah,R., Wang,X., Xhemalce,B., Wood,A.D., Green,A.R., Gottgens,B. *et al.* (2012) Three distinct patterns of histone H3Y41 phosphorylation mark active genes. *Cell Rep.*, **2**, 470–477.
59. Tropberger,P., Pott,S., Keller,C., Kamieniarz-Gdula,K., Caron,M., Richter,F., Li,G., Mittler,G., Liu,E.T., Buhler,M. *et al.* (2013) Regulation of transcription through acetylation of H3K122 on the lateral surface of the histone octamer. *Cell*, **152**, 859–872.
60. Lee,J.H., Kang,B.H., Jang,H., Kim,T.W., Choi,J., Kwak,S., Han,J., Cho,E.J. and Youn,H.D. (2015) AKT phosphorylates H3-threonine 45 to facilitate termination of gene transcription in response to DNA damage. *Nucleic Acids Res.*, **43**, 4505–4516.
61. Rapkin,L.M., Ahmed,K., Dulev,S., Li,R., Kimura,H., Ishov,A.M. and Bazett-Jones,D.P. (2015) The histone chaperone DAXX maintains the structural organization of heterochromatin domains. *Epigenet. Chromatin*, **8**, 44.
62. Udugama,M., M Chang,F.T., Chan,F.L., Tang,M.C., Pickett,H.A., R McGhie,J.D., Mayne,L., Collas,P., Mann,J.R. and Wong,L.H. (2015) Histone variant H3.3 provides the heterochromatic H3 lysine 9 tri-methylation mark at telomeres. *Nucleic Acids Res.*, **43**, 10227–10237.
63. Edgar,R., Domrachev,M. and Lash,A.E. (2002) Gene Expression Omnibus: NCBI gene expression and hybridization array data repository. *Nucleic Acids Res.*, **30**, 207–210.
64. Timms,R.T., Tchasovnikarova,I.A., Antrobus,R., Dougan,G. and Lehner,P.J. (2016) ATF7IP-mediated stabilization of the histone methyltransferase SETDB1 is essential for heterochromatin formation by the HUSH complex. *Cell Rep.*, **17**, 653–659.
65. Bailey,T.L. and Elkan,C. (1994) Fitting a mixture model by expectation maximization to discover motifs in biopolymers. *Proc. Int. Conf. Intel. Syst. Mol. Biol.*, **2**, 28–36.